Multi-Objective Whale Optimization Algorithm for Balance Recovery of a Humanoid Robot

Kittisak Sanprasit and Pramin Artrit
Dept. Electrical Engineering, Faculty of Engineering, Khon Kaen University, Khon Kaen, Thailand
Email: kittisak.san@lru.ac.th, pramin@kku.ac.th

***Abstract*— In the near future, the humanoid robot has been expected to associate and work with a human. There is a chance that it has been hit from an external force and the robot cannot keep its balance. Thus, the robot might falls to human causing casualty or if it falls down to the ground the damage could cause ultimately to itself. For this reason, the humanoid must have balance recovering processes for protecting itself from the external force to prevent such damage. Therefore, this research proposes an optimal path design for a stand-balancing humanoid robot. The experiment simulates this situation using a force 1.11N hits to the humanoid (Bioloid Premium Type A) robot. This commercial humanoid robot has 18 Degree of Freedoms (DOFs). With this complexity of DOFs, the mathematical model and joints control strategies are investigated to restore robot balancing. Six strategies are chosen to implement in this work; 1) ankle strategy, 2) knee strategy, 3) ankle and knee strategy, 4) ankle and hip strategy, 5) ankle knee and hip strategy, and 6) whole body (ankle, knee, hip, arms) strategy using Multi-objective Whale optimization algorithm (MOWOA) together with non-dominated solution and decision making by weighted product method. Three objective functions are employed; 1) a minimal orbital energy, 2) a minimal error of phase portrait, and 3) a minimal jerk. The results have shown that the ankle strategy gives the best result based on decision making by the weighted product method.**

***Index Terms*— Humanoid Robot, MOWOA, weighted product method, Pareto front, Balancing, objective functions**

I. Introduction

The robot with two-legs moving that consisted of a mechanism like the human body is called “Humanoid Robot” composed of two legs, two arms, body (torso) and head. They recently received much interest in conducting many types of research, such as modeling, stability, walking patterns, running, jumping [1-4], etc. Also, humanoid robots have also been used for home facilitation [5] or industrial applications [6]. In the near future, the humanoid robot is expected to associate and work with a human. There is a chance that it has been hit from an external force and the robot cannot keep its balance. Thus, the robot might falls to human causing casualty or if it falls down to the ground the damage could cause ultimately to itself, for example, the impact force from human and animals which affected on humanoid robots resulted in their inability to maintaining balance. For this reason, they could fall down on the ground that ultimately resulted in robot damage. Many researchers have studied and developed an appropriate method to maintain robot balancing from the external force with ankle strategy, hip strategy, step-out [7] and two-step [8], etc. However, the step-out method to maintain robot balance is effective in a smooth area without any obstacle. , but sometimes the environment such as stairs, rough areas, etc. may not provide convenience in stepping to maintain balancing. Many researchers have tried to find the way to increase the effectiveness of maintaining balance without stepping such as ankle and knee strategy [9], ankle and hip strategy [10], arm rotation strategy [11], etc. The control strategy of various joints affected to the robot’s Center of Mass (COM). Each joint carries different load depend on where it is located. This causes different in the speed. For example, the ankle takes most body weight, during a standing gesture thus it becomes the slowest joint. The consequences is that the COM movement gives slow response and leads to less stability in the robot.

The work compares between six strategies that are; 1) ankle strategy, 2) knee strategy, 3) ankle and knee strategy, 4) ankle and hip strategy, 5) ankle, knee and hip strategy, and 6) whole body (ankle, knee, hip and arms) strategy. This work also proposed a multi-objective optimization to determine the balance recovery trajectory. Three objective functions are employed i.e. minimal orbital energy to ensure that the robot can return to balance as soon as possible, the minimal error of phase portrait for the smooth movement of COG position in phase portrait, and minimal jerk to prevent damage from joint equipment. With these objective functions together with Whale optimization, this work proposes the Multi-objective Whale optimization algorithm (MOWOA). This is a new meta-heuristic optimization algorithm [12]. In 2016, Thi-Kien Dao, Tien-Szu Pan, and Jeng-Shyang Pan [12] applied a multi-objective Whale Optimization Algorithm (MOWOA) to optimal mobile robot path planning. In 2017, Jianzhou Wang, Pei Du, Tong Niu, Wendong Yang [13] used a multi-objective Whale Optimization Algorithm for wind speed forecasting. They also utilize a non-dominated solution for Pareto front. The selection of the optimum point of Pareto front use the decision making employs minimal weighted product method (WPM) [14]. Next, the best optimum point result

Manuscript received July 21, 2019; revised April 4, 2020.

doi: 10.18178/ijmerr.9.6.882-893

is implemented on the real humanoid robot. Finally, the experiment compared results on the real robot applying angle from trial-and-error and MOWOA techniques.

This paper is arranged as follows: starting with introduction, Section 2 presents the humanoid robot modeling. Section 3 shown numerical simulation while its results and experimental is shown in Section 4. The work ends with conclusion in Section 5.

II. HUMANOID ROBOT MODELING

A. Kinematics Model

The kinematics consisted of 2 types which are 1) forward kinematics or direct kinematics and 2) inverse kinematics [15]. The forward kinematics problem is the relationship between the operational coordinates of a robot on the Cartesian coordinate frame (x,y,z). It can analysis stability of robot. In this research, the forward kinematics use Denavit-Hartenberg (DH) [15]. It is proposed a general method to describe the structure of a robot.

A DH coordinate frame is defined by four parameters: θ_i, d_i, a_i, and α_i represents of joint angle, joint distance, link length, and link twist, respectively. All variables in each frame created as a table called "DH parameter table".

This research uses the Bioloid premium Type A. In 2012, J. Victor Nunez [16] invented inverse kinematics of 18 joints. A model of the robot developed from the Computer Aided Design (CAD) model provided by the manufacturer ROBOTIS. In 2013, J. Ramon Cerritos-Jasso [17] developed forward kinematics of 12 joints, considered only the legs, since it used for the gait cycle analysis for soccer robot competition FIFA 2013.

The DH parameter table used to calculate the movement of each frame for each joint by applying homogeneous transformation matrix (1) to explain the rotation and sliding of each link according to the equation as follows [15] [18].

$$^{i-1}T_i = Rot_{z,\theta_i} Trans_{z,d_i} Trans_{x,a_i} Rot_{x,\alpha_i}$$

$$^{i-1}T_i = \begin{bmatrix} C_{\theta_i} & -S_{\theta_i} & 0 & 0 \\ S_{\theta_i} & C_{\theta_i} & 0 & 0 \\ 0 & 0 & 1 & 0 \\ 0 & 0 & 0 & 1 \end{bmatrix} \begin{bmatrix} 1 & 0 & 0 & 0 \\ 0 & 1 & 0 & 0 \\ 0 & 0 & 1 & d_i \\ 0 & 0 & 0 & 1 \end{bmatrix} \begin{bmatrix} 1 & 0 & 0 & a_i \\ 0 & 1 & 0 & 0 \\ 0 & 0 & 1 & 0 \\ 0 & 0 & 0 & 1 \end{bmatrix} \begin{bmatrix} 1 & 0 & 0 & 0 \\ 0 & C_{\alpha_i} & -S_{\alpha_i} & 0 \\ 0 & S_{\alpha_i} & C_{\alpha_i} & 0 \\ 0 & 0 & 0 & 1 \end{bmatrix}$$

$$= \begin{bmatrix} C_{\theta_i} & -S_{\theta_i}C_{\alpha_i} & S_{\theta_i}S_{\alpha_i} & a_iC_{\theta_i} \\ S_{\theta_i} & C_{\theta_i}C_{\alpha_i} & -C_{\theta_i}S_{\alpha_i} & a_iS_{\theta_i} \\ 0 & S_{\alpha_i} & C_{\alpha_i} & d_i \\ 0 & 0 & 0 & 1 \end{bmatrix} \text{when} \begin{matrix} S_{\theta_i} = sin(\theta_i) & , & C_{\theta_i} = cos(\theta_i) \\ S_{\alpha_i} = sin(\alpha_i) & , & C_{\alpha_i} = cos(\alpha_i) \end{matrix} \quad (1)$$

Fig. 1, shows the variables of Bioloid robot for forward kinematics by Denavit-Hartenberg in the calculation of COM of the robot. The initial position at the outer left heel as a starting point (A). While end effector F, H, R, and L represents of foot left heel, head, end of the right arm, and end of the left arm, respectively. The center of mass each link (Pcomi) of the robot has 11 parts (i=1,2,..,11) and the calculation position of COM of the robot (Pcom) shown in Fig. 1, and the position of foot sole rotation also shown in Fig. 2.

The position of center mass each link uses a measurement device, the researcher a development of the Center of Gravity (COG) measurement device for the center of each link. This device consists of 4 strain gauges placed on each glass plate's corner, size 300x300 mm^2. It can carry a weight of less than 5 kg. The output demonstrates by weight and locates COG in a coordinate (x, y) as shown in Fig. 3. The experiment would be conducted 2 times by changing the direction of the mass center of each side that resulting in receiving the position of the mass center for all 3 planes (x,y,z).

Then the DH parameter table is created and categorized into 3 parts. The first DH parameter of the virtual joint (V) which was not a real joint of the robot, but it is just a virtual joint used in the movement of front foot angle, heel angle, and body as shown in Fig. 2. The DH parameter is shown in Appendix Table A.1, A.3. The second part is the DH parameter table joints of robot as shown in Appendix A.2, A.4, A.5, and the third part is DH parameter table of mass each link to consist of right ankle mass (M1), right knee mass (M2), right hip mass (M3), left hip mass (M4), left knee mass (M5), left ankle mass (M6), upper body mass (M7), right shoulder joint mass (M8), right elbow mass (M9), left shoulder joint mass (M 10) and left elbow mass (M 11) shown in Appendix Table A.6 and show values of variables in Appendix B (Table B).

The calculation from the initial reference position (A) to the end effector of the robot apply homogeneous transformation matrix (1). The end effector of the robot consists of F, H, R, and L represent, and the center of mass each link (Pcomi) of the robot. The homogeneous transformation matrix was shown as follows.

The transformation matrix between the initial reference frame (A) and the joint angle of right ankle (V) is derived as:

$$^0T_{V5} = {}^0T_{V1}\, {}^{V1}T_{V2}\, {}^{V2}T_{V3}\, {}^{V3}T_{V4}\, {}^{V4}T_{V5} \quad (2)$$

The transformation matrix between the initial reference frame (A) and the joint angle of right hip (q6) is derived as:

$$^0T_6 = {}^0T_{V5}\, {}^{V5}T_1\, {}^1T_2\, {}^2T_3\, {}^3T_4\, {}^4T_5\, {}^5T_6 \quad (3)$$

The transformation matrix between the initial reference frame (A) and the foot left heel (F) is derived as:

$$^0T_{14} = {}^0T_6\, {}^6T_7\, {}^7T_8\, {}^8T_9\, {}^9T_{10}\, {}^{10}T_{11}\, {}^{11}T_{12}\, {}^{12}T_{13}\, {}^{13}T_{14} \quad (4)$$

The transformation matrix between the initial reference frame (A) and each end effector of H, R, and L can repeat according to (4). Next, The calculation from the initial reference position (A) to the center of mass each link (Pcomi) of the robot. The transformation matrix was shown as follows.

The transformation matrix between the initial reference frame (A) and the COM of left hip (Pcom4) is derived as:

$$^0T_{C6} = {}^0T_{V5}\, {}^{V5}T_1\, {}^1T_2\, {}^2T_3\, {}^3T_4\, {}^4T_5\, {}^5T_6\, {}^6T_7\, {}^7T_8\, {}^8T_9\, {}^9T_{C5}\, {}^{C5}T_{C6} \quad (5)$$

The transformation matrix between the initial reference frame (A) and the center of mass each link (Pcomi) (i=1,2,3,5,..,11) of the robot can be obtained similar to (5).

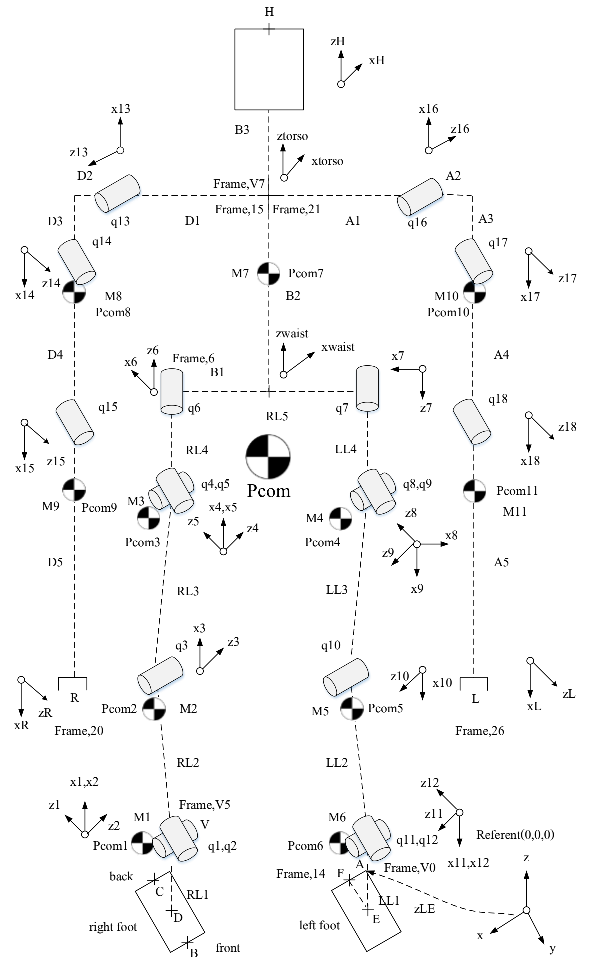

Figure 1. Parameter of Humanoid robot Bioloid premium Type A.

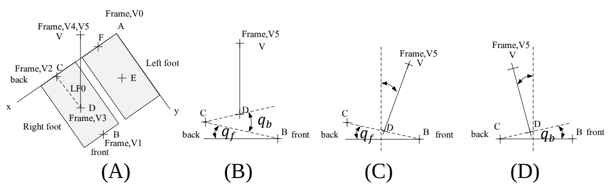

Figure 2. The position of foot for rotation; (A) position reference frame to the joint of right ankle, (B) rotation bend to the front and back, (C) rotation bend to the front (D) rotation bend to the back.

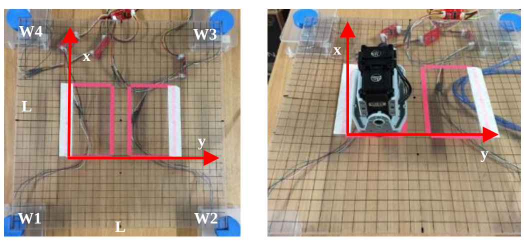

Figure 3. The four weight scales for calculation COM.

B. Center of Mass (COM) of robot

The position of the mass of each link was calculated to find the position COM of the robot in the rectangular coordinate frame as follows [2].

$$P_{com} = \frac{\sum_{i=1}^{n} m_i P_i}{\sum_{i=1}^{n} m_i}$$

When P_{com}, m_i, P_i represent of position COM of the robot, a mass of each link, and position in the Cartesian coordinate frame of mass each link, respectively.

C. Linear Inverted Pendulum Model (LIPM)

The humanoid robot is a system with complex dynamics. It is useful to approximate these dynamic by a simple model. The simple model used in this research is the Linear Inverted Pendulum Model (LIPM) [10] as shown in Fig. 4(A). The calculation of the acceleration axis y of the robot was shown as follows.

$$\ddot{Y}_{COG} = \frac{g}{ZG_C}(Y_{COG} - Y_{COP}) = \omega_0^2(Y_{COG} - Y_{COP}) \quad (7)$$

With $\ddot{Y}_{COG}$, g, ZG_C, Y_{COG}, Y_{COP}, and $\omega_0 = \sqrt{\frac{g}{ZG_C}}$ represent of acceleration, gravitational constant, the constant height of COM, the position Center of gravity (COG) in axis y, position of Center of pressure (COP), and time constant of a single pendulum, respectively.

D. Center of Pressure (COP)

The COP is the point of application of the resultant ground reaction force of the robot. The COP should stay within the convex hull of the foot support area, can be rewritten as.

$$Y_{COP} = Y_{COG} - \left(\frac{ZG_C}{g}\right)\ddot{Y}_{COG} = Y_{COG} - \left(\frac{\ddot{Y}_{COG}}{\omega_0^2}\right) \quad (8)$$

This constraint is written as follows, $l_r < Y_{COP} < l_f$ which l_r and l_f represent of rear-foot-edge and front-foot-edge, respectively. The COP is used to calculate orbital energy in objective functions.

E. Balancing Humanoid Robot

The balancing of human for clockwise and counterclockwise apply the relationship between COG and COP [19]. Many researchers employs this relation to the balance recovery process using the combination from various joint movements. For example, S.Kiemel [10] applied Ankle strategy and Ankle-Hip strategy to balance recovery for the Tulip robot. To keep the Sarcos Primus robot balance, Benjamin Stephens [20] employed the Step-out strategy. In this research, the relationship between COG and COP for balancing is demonstrated in Fig. 4.

Each figure shows the changing situation at one of six different points in time. Time-1 (see Fig. 4(A)), the robot standing with the reference position situated on the robot left heel and received external force at the upper body. At this position, COP = COG, and angle of the foot sole which refers to the floor is set to 0. Next, the heel would be rotated, and the robot would move to the rear which affected to position of COG leads COP according to the direction of external force or this position, COP > COG in referent and the angle of foot > 0, such that at Time-2 (see Fig. 4(B)). At Time-3 (see Fig. 4(C)), the robot response balance recovery by joints of the robot, to slide COP position ahead of COG position or this position, COP < COG in referent. After that, the robot would stay still for a moment at this position, Time-4 as shown in Fig. 4(D). Later, the robot would bring the joint position to the initial position at Time-5, as shown in Fig. 4 (E). Finally, the robot would landed freedom by the gravity to forward at Time-6 as shown in Fig. 4 (F).

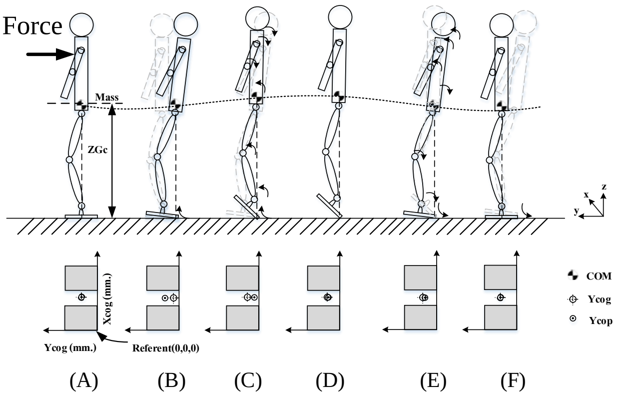

Figure 4. The stand-balancing humanoid robot from external force. (A) the robot standing, (B) the robot would move to the rear, (C) the robot response balance recovery by joints of robot, (D) the robot would stay still, (E) the joint position at the initial position, (F) the robot to forward.

F. Trajectory

This research uses the trajectory of cubic spline interpolation in two trajectories: the trajectory of COG and the trajectory of the joint of a robot. The velocity and acceleration of the initial and final conditions are specified to be zero. The interval time of cubic spline interpolation $[t_i, t_{i+1}]$ [21, 22] can be rewritten as:

Position :

$$Q_{j,i}(t) = \frac{\ddot{Q}_{j,i}(t_i)}{6h_i}(t_{i+1}-t)^3 + \frac{\ddot{Q}_{j,i}(t_{i+1})}{6h_i}(t-t_i)^3 + \left(\frac{q_{j,i}}{h_i} - \frac{\ddot{Q}_{j,i}(t_i)}{6}h_i\right)(t_{i+1}-t) + \left(\frac{q_{j,i+1}}{h_i} - \frac{\ddot{Q}_{j,i}(t_{i+1})}{6}h_i\right)(t-t_i) \quad (9)$$

Velocity :

$$\dot{Q}_{j,i}(t) = -\frac{\ddot{Q}_{j,i}(t_i)}{2h_i}(t_{i+1}-t)^2 + \frac{\ddot{Q}_{j,i}(t_{i+1})}{2h_i}(t-t_i)^2 - \left(\frac{q_{j,i}}{h_i} - \frac{\ddot{Q}_{j,i}(t_i)}{6}h_i\right) + \left(\frac{q_{j,i+1}}{h_i} - \frac{\ddot{Q}_{j,i}(t_{i+1})}{6}h_i\right) \quad (10)$$

Acceleration :

$$\ddot{Q}_{j,i}(t) = \frac{\ddot{Q}_{j,i}(t_i)}{h_i}(t_{i+1}-t) + \frac{\ddot{Q}_{j,i}(t_{i+1})}{h_i}(t-t_i) \quad (11)$$

Jerk :

$$\ddot{Q}_{j,i}(t) = \frac{\ddot{Q}_{j,i}(t_{i+1}) - \ddot{Q}_{j,i}(t_i)}{h_i} \quad (12)$$

The condition in velocity, acceleration of the initial and final are specified to be zero and continuous. Therefore, two extra knots (position ($\bar{q}_2$, $\bar{q}_{n-1}$) at time ($\bar{t}_2 = \frac{t_1+t_3}{2}$, $\bar{t}_{n-1} = \frac{t_{n-2}+t_n}{2}$) [18,19], can be rewritten as.

$$\bar{q}_2 = q_1 + h_1 v_1 + \frac{h_1^2}{3}a_1 + \frac{h_1^2}{6}\ddot{Q}_{j,2}(t_2) \quad (13)$$
$$\bar{q}_{n-1} = q_n - h_{n-1}v_n + \frac{h_{n-1}^2}{3}a_n + \frac{h_{n-1}^2}{6}\ddot{Q}_{j,n-1}(t_{n-1})$$

When $Q_{j,i}(t)$, $h_i = t_{i+1} - t$, $q_{j,i}$, $\ddot{Q}_{j,i}(t)$, v_1, v_n, a_1, a_n, j and i represent of position, interval time, position of joint, acceleration of joint, initial velocity, final velocity, initial acceleration, final acceleration, a joint of robot and a knot sequences, respectively. In the case of the trajectory COG position without j variable.

III. Numerical Simulation

The numerical simulation present step by step procedure of implementation of the proposed numerical simulation is outlined below as shown in Fig. 5.

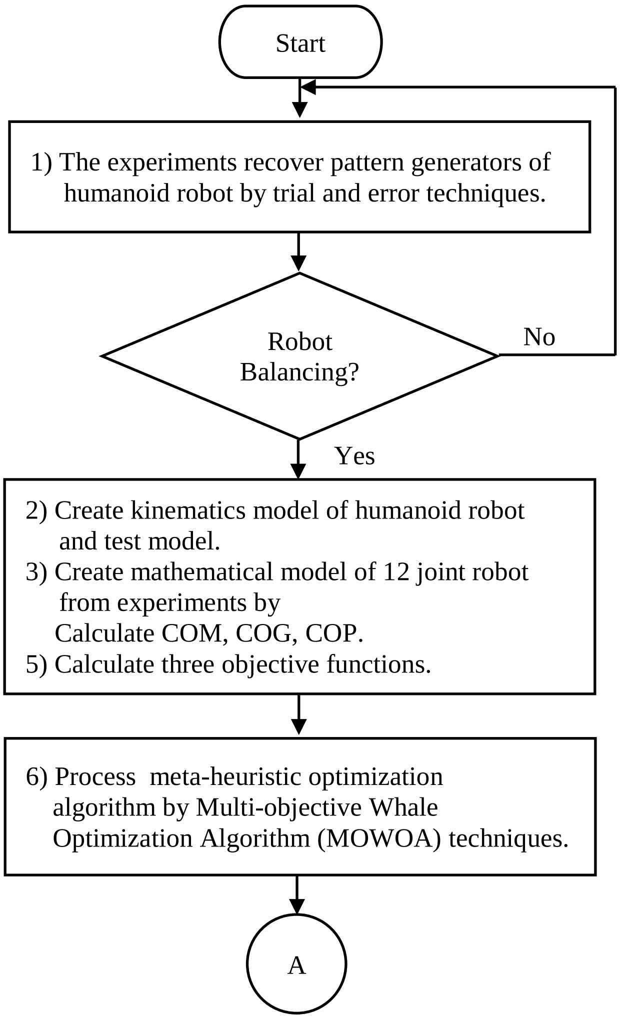

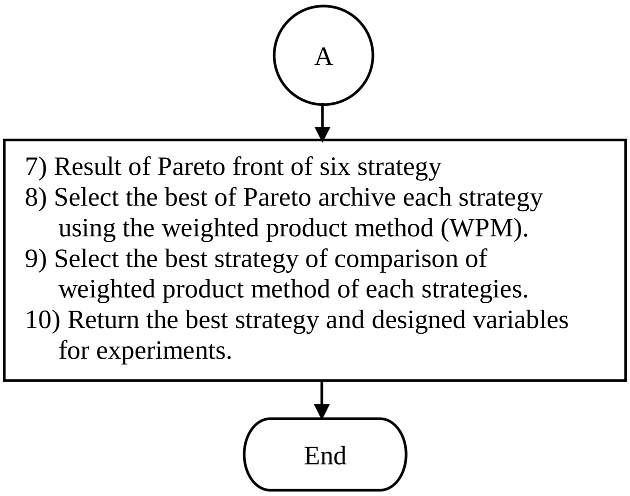

Figure 5. The process of numerical simulation.

A. Multi-objective of Balancing Humanoid Robot

The multi-objective optimization is a design assigned to determine optimal point. For the problem that has more than one objective functions, it also has more than one optimum solution. The traditional combination of these results is called a set of Pareto optimal solutions or a Pareto front which is viewed in the objective function domain.

A typical mathematical formulation of multi-objective optimization can be expressed as:

$$Mimimize : F(x) = \{f_1(x), f_2(x), \ldots, f_o(x)\} \quad (14)$$

Constraints

$$g_i(x) \leq 0, i = 1, \ldots, m$$
$$h_i(x) = 0, i = 1, \ldots, l$$
$$L_i \leq x_i \leq U_i, i = 1, \ldots, n$$

When x and f_i represents of design variable and objective functions, respectively. Function $g_i(x)$ and $h_i(x)$ are the inequality and equality constraints while L_i and U_i are lower and upper bound constraints. Parameter m, l, and n are number of variable and o is number objective function.

A.1 Objective functions

The design problem in this study has three objective functions which are the minimum orbital energy $(E_{LIPM,Y})$, minimum error of phase portrait (r_{error}), and the minimum jerk$(jerk)$. Details can be descripted as follows.

A.1.1 Orbital energy minimization

Concept of the orbital energy is conserved in the motion of the simplified humanoid robot model which is considered as a Linear Inverted Pendulum [23]. S. Kajita, et al. applied it to observe the humanoid balancing [23]. The total energy is determined in (15) and the objective function in (16).

$$E_{LIPM,Y} = constant = \frac{1}{2}\dot{Y}_{COG}^2 - \frac{g}{2ZG_C}(Y_{COG} - Y_{COP})^2 \quad (15)$$

$$FOBJ1 = min \sum_{t_0}^{t_{end}} \left|E_{LIPM,Y}(t)\right| \quad (16)$$

To ensure that the robot recovering its balance, the COG position is manipulated to be the original position as before it has been hit. Not only the position but also the velocity of the COG are considered. If the velocity is not 0, the robot cannot assume to be recovered. Therefore, the COG's phase portrait is introduced [10][20]. It is a contour of the COG position versus it's velocity, see Fig. 6.

A.1.2 Error of phase portrait minimization

The smoothness of this path represents smoothness of the robot movement. In this work, the standard ellipse path is set as the deigned path of the COG's phase portrait. The COG path, in this work, is also called the ellipse based trajectory. Error between the standard ellipse and the ellipse based trajectory present on proportional of position and velocity of the COG. Large error can lead to difficulty of bringing the robot's trajectory to it's balance.

Its center position (x_{center}, y_{center}) of COG path is derived as:

$$x_{center} = x_{min} + \left(\frac{x_{max} - x_{min}}{2}\right)$$
$$y_{center} = y_{min} + \left(\frac{|y_{max}| + |y_{min}|}{2}\right)$$

Where (x_{min}, y_{min}) and (x_{max}, y_{max}) represent the minimum and maximum of position standard ellipse, respectively.

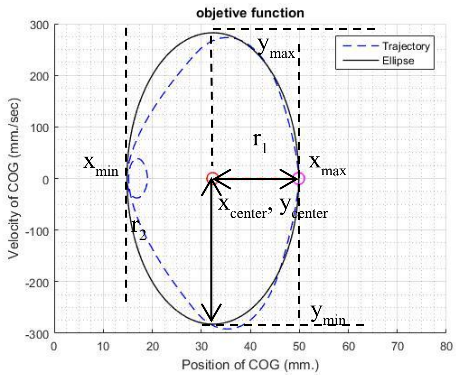

Figure 6. Ellipse based trajectory of COG in the phase portrait.

The calculation error of radius (r_{error}) is derived as:

$$r_{ellipse}(t) = \sqrt{x_{ellipse}^2(t) + y_{ellipse}^2(t)}$$
$$r_{cog}(t) = \sqrt{x_{cog}^2(t) + y_{cog}^2(t)}$$
$$r_{error}(t) = \left|r_{ellipse}(t) - r_{cog}(t)\right|$$

When $(x_{ellipse} = r_1 \cos\theta + x_{center}, y_{ellipse} = r_2 \sin\theta + y_{center})$, (x_{cog}, y_{cog}), $r_{ellipse}$, r_{cog}, $r_1 = x_{max} - x_{center}$ and $r_2 = y_{center}$ represent the position standard ellipse, position of COG, radius of standard ellipse and radius of COG, radius of standard ellipse axis x and radius of standard ellipse axis y, respectively and the objective function in (17).

$$FOBJ2 = min \sum_{t_0}^{t_{end}} r_{error}(t) \tag{17}$$

Jerk in particular is related with mechanical wear off. The systems are considered jerk monitoring are specially useful for protective supervision. Thus, it may minimize the sum of the squared jerk along its trajectory to objective function.

A.1.3 Jerk minimization

In this work, the servo motors are applied for the robot's joints, therefore, the system should have a minimum jerk, see (12), and objective function presents in (17) [24].

$$FOBJ3 = min \sum_{j=1}^{N} \int_{t_0}^{t_{end}} |\dddot{q}(t)| dt \tag{18}$$

The inequality and equality determined constraints for balance recovery as:

$$0 \le q_j \le 20$$
$$|\dot{q}_j(t)| = v_{maxj}$$
$$|\dddot{q}_j(t)| \le JC_j$$

Where v_{maxj} and JC_j represents of maximum velocity of the joint angle and jerk constraints of third quartile (Q3) of the statistics boxplot. The lower bound and upper bound are set to 0 degree and 20 degree for the range of each joint.

B. Multi-Objective Whale Optimization Algorithm

Multi-objective Whale Optimization Algorithm (MOWOA) is a recent meta-heuristic optimization algorithm proposed by Ishwar Ram Kumawat, et al. [25]. In this work, apply optimization techniques search optimum point for balance recovery. Their solutions are unlikely to give premature convergence. They also utilize non-dominated solution for Pareto front [25][26].

B.1 Multi-objective

An external Pareto archive employs a non-dominated solution. The step by step procedure of implementation of the proposed algorithm is outlined below:

Step 1: Initialize population of design variable vector is set as the joint angle value related to the chosen strategy.

$$Q = \begin{bmatrix} q_1 \\ q_2 \\ \vdots \\ q_n \end{bmatrix} = \begin{bmatrix} q_{1,1} & \cdots & q_{1,d} \\ q_{2,1} & \cdots & q_{2,d} \\ \vdots & \cdots & \vdots \\ q_{n,1} & \cdots & q_{n,d} \end{bmatrix}, \ 0 \le q \le 20 \tag{19}$$

When q is the value of joint angle range 0-20 degree. The angle is picked randomly and then roundup to the possible value of the Bioloid's angle. The servo motor of the robot has a resolution of 0.29 degree. The subscript n is the population size or number of search agents and d indicates the number of joints in the chosen strategy. For example, the number d of the "ankle" or "knee" strategies is 2, the "ankle and knee" or "ankle and hip" strategies is 4. In the case of "ankle, knee and hip" and the whole body (ankle, knee, hip, arms), d is 6 and 12, respectively.

Step 2: Evaluate the fitness evaluation of a design variable vector. For the three objectives f_1, f_2, f_3 and the vector solution, F is feasible solutions in inequality constraints.

$$F(Q) = \begin{bmatrix} f_1(q_1) & f_2(q_1) & f_3(q_1) \\ f_1(q_2) & f_2(q_2) & f_3(q_2) \\ \vdots & \cdots & \vdots \\ f_1(q_n) & f_2(q_n) & f_3(q_n) \end{bmatrix} \tag{20}$$

Step 3: Determine the non-dominated solution (NS) as shown in Fig. 7. They store and update a set of non-dominate in Pareto archive (P).

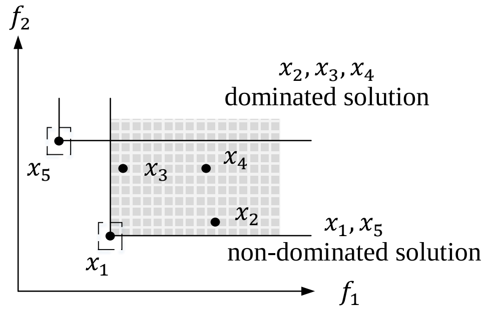

Figure 7. Non-dominated solutions.

Step 4: Select the best solution from Pareto archive using the roulette wheel technique and grid mechanism [27].

Step 5: Update the best solution if there are better solutions then the next generation is generated.

Step 6: Repeat step 1 to 5 until a termination criterion is met.

B.2 Multi-Criteria Decision Making (MCDM) methods

To select the best Pareto archive, the MCDM method, the weighted product method (WPM) is utilized. The multi-criteria utility function (U) is introduced [14] by multiplying all three of the objective function values, see (21).

$$U = \prod_{i=1}^{n} \left[F_i(x)\right]^{w_i} \tag{21}$$

Where n is a number of the objective function and the w_i is the weights indicating the relative importance of the objective functions [14], called weight index.

C. Whale Optimization Algorithm (WOA)

The WOA algorithm is an optimization mimicking the hunting behavior of the humpback whale. The searching pattern imitates an encircling prey, spiral bubble-net feeding maneuver, and searches for prey [28].The Pseudo code of the WOA is shown in Fig. 8.

This investigation is conducted utilize the MATLAB software. All variable, parameters, and their values are defined as follow: the population size or number of search agents (n_a) = 30, number of population = (2,4,6,12), number of iteration (n_{iter}) = 100, size of Pareto archive ($n_{archive}$) = 300, number of grid per each dimension (nGrid) = 10, grid inflation parameter(alpha) = 0.1, vector $\vec{\alpha}$ from 2 to 0, lower bound constraints(L_i)= 0, upper bound constraints (U_i) = 20, weight index (w_i) =1. Each strategy accomplished by 5 independent runs.

```
Pseudo code : WOA (Algorithm)
Initialize the whales population Xi (i=1,2,…n)
Calculate the fitness of each search agent
X* the best search agent
while (t<maximum number of iterations)
      for each search agent
          Update a,A,C,l,and P
          if1(P<0.5)
             if2(|A|<1)
                 Update the position of the current search agent
             else if2(|A|≥1)
                 Select a random search agent (Xrand)
                 Update the position of the current search agent
             end if2
          else if1(P≥0.5)
                 Update the position of the current search agent
          end if1
      end for
      Check if any search agent goes beyond the search space and
amend it
       Calculate the fitness of each search agent
       Update X* if there is a better solution
       t=t+1
end while
return X*
```

Figure 8. Pseudo code of the WOA algorithm [28].

D. Simulation Result

The Pareto front of six strategies are illustrated in Fig. 9, and the minimization WPM for each strategy is presented in TABLE 1. The ankle strategy gives the best result for the WPM which is 617,187,582,559,110.00. The first objective function (Orbital Energy) is 3,219,129.50, and the second objective function (error of phase portrait) is 4,046.05579 mm^2/s. In addition, the third objective function which is the total jerk of left and right ankle is 47,385.65234 deg/sec^3. The movements of the robot using the ankle strategy for step balancing is shown in Fig. 10. The designed variable is the ankle strategy which had the angle joint = 4.93 degree.

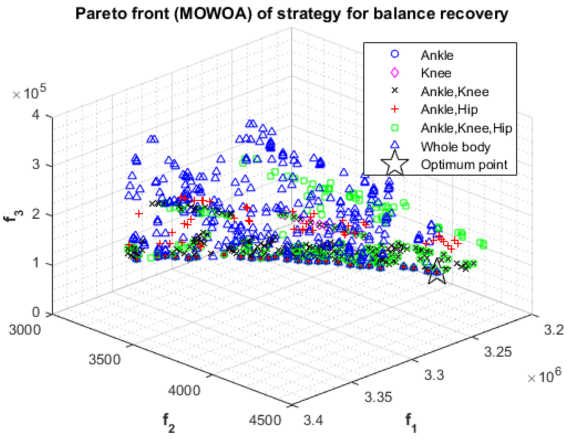

Figure 9. Pareto front 3 objective functions (f_1,f_2,f_3).

TABLE I. MINIMIZATION VALUE OF WPM FOR EACH STRATEGY

Strategy	Best (minimization weighted product)	Design variable
ankle	**617,187,582,559,110.00**	q_{Ankle}=4.93
knee	1,175,460,976,818,350.00	q_{Knee} =9.28
ankle and knee	**617,187,582,559,110.00**	q_{Ankle}=4.93 q_{Knee}=0
ankle and hip	**617,187,582,559,110.00**	q_{Ankle}=4.93 q_{Hip}=0
ankle, knee and hip	**617,187,582,559,110.00**	q_{Ankle}=4.93 q_{Knee}=0 q_{Hip}=0
whole body (ankle,knee,hip,arms)	**617,187,582,559,110.00**	q_{Ankle}=4.93 q_{Knee}=0 q_{Hip}=0 $q_{shoulder1}$=0 $q_{shoulde2}$=0 q_{elbow}=0

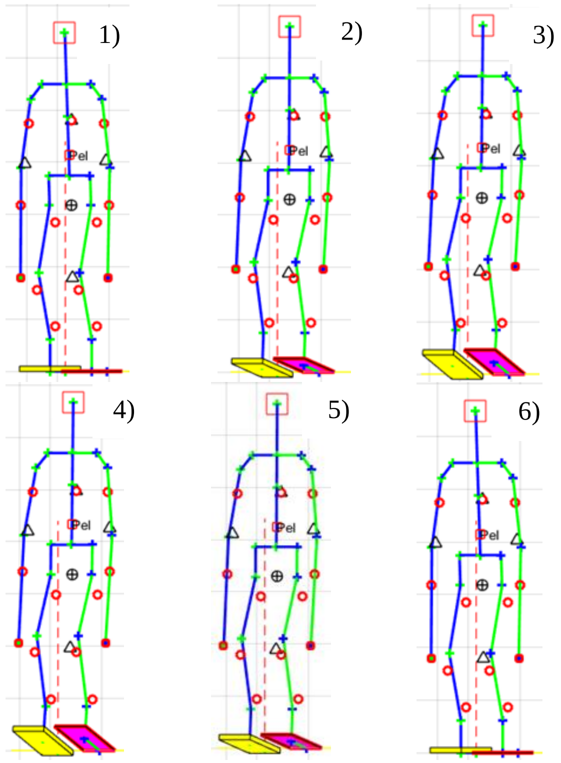

Figure 10. The simulation of stand-balancing humanoid robot from external force by Ankle strategy.

IV. Experimental

From the previous section, the simulation shows that the Ankle strategy achieves the best optimum point. Next step, the simulation results are implemented on the real humanoid robot.

A. Experimental Setup

This work uses the Bioloid premium Type A for all experiments. It is 350 mm tall, weight 1.736 kg, foot size is width 60 mm and length 100 mm. The left and right foot is apart for 20 mm. During the double-support phase (DSP), the stable region, inside 2 feet, is 140 mm x 100 mm The center of mass of this robot locates at (70 mm, 50 mm, 159 mm), where the origin point (reference point) is on the outer heel of the left foot, shown in Fig 1. An external force is generated from a 0.5 kg iron weight tighten to a 225 mm cable and is pulled the string to an angle of 27.5 degree, such pendulum provides centripetal force (F_{net} = 1.11 N) or Impulse (Id=0.352 Ns).

In addition, the balancing is described as follows. The robot would stand still to maintain balancing that it stood upright with slightly bended knee in order to make the COM position placed in the middle of the feet. The robot system would keep joint position at the initial position (home position) and then the external force hit the robot on the upper front area, height of 254 mm see Fig. 11(A). The main control unit for all 18 servo-motors is the CM-530 module through the RS232 communication protocol. The joint angle is acquired from CM-530 and send to MATLAB program. Only two joint angles are needed for an Ankle strategy, this makes the average sampling rate to 52.35 Hz. The robot's left foot consists of a 9-axis sensor (MPU9150). It provides the angle of the foot sole which refers to the floor. Another one PC is dedicated the fetch the angle data from MPU9150 to the MATLAB with sampling rate of 26.59 Hz.

B. Ankle Strategy for Balancing

As the simulation result indicates that the Ankle strategy gives the best optimum point, the controlled joint angle of right (q2) and left (q11) are set to 4.93 degree. At this state, the toe is lifted and sole product a 13.482 degree to the floor. Movements of the robot are demonstrated in Fig. 11. The process of restoring robot's balance can be divided into 6 periods. First period, before an external force hit, the robot stands balance in the initial position, see Fig. 11(A). Second period, right after the robot has been hit, the robot is moved to the rear, same direction of the force, Fig. 11(B). Third period, ankle joints are controlled to 4.93 degree while an soles angle are slightly increased, as show in Fig. 11(C). After that, the robot would stay still for a moment as shown in Fig. 11(D). Next, it would adjust the joint position at the initial position as shown in Fig. 11(E). Finally, the robot body is moved forward by the gravity and landed to the ground for balancing, as shown in Fig. 11(F). The results of the restoring balance is reported in Table II.

TABLE II. The Result of Restoring Balance Process.

step	Time (sec)	Angle of foot (degree)	Ankle joints (degree)
1	0	0	0
2	0.131	7.454	0
3	0.318	13.482	4.93
4	0.470	13.482	4.93
5	0.728	7.454	0
6	0.878	0	0

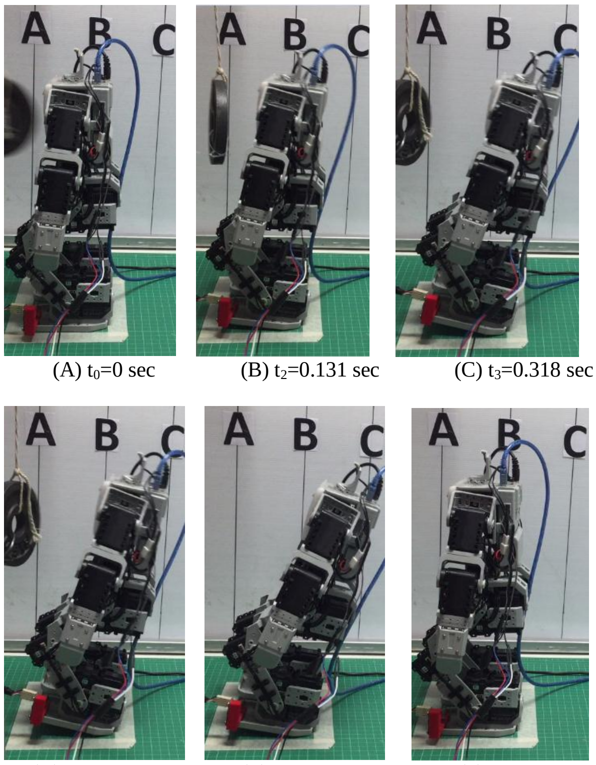

(A) t_0=0 sec (B) t_2=0.131 sec (C) t_3=0.318 sec

(D) t_4=0.470 sec (E) t_5=0.728 sec (F) t_6=0.878 sec

Figure 11. The experimental of stand-balancing humanoid robot from external force.

C. Results and Analysis

Three experimentation results are compared; 1) the result from trial-and-error technique, 2) the result from the best of optimum point simulation of Ankle strategy by MOWOA and 3) the actual result using the value from the simulation. The robot can restore it's balance for these three experiments. Average error angle of foot = 1.813 degree (13.448%) (see Fig. 12), right ankle (q2) = 0.747 degree (15.154%) (see Fig. 13), left ankle (q11) = 0.852 degree (17.294%) (see Fig. 14). The results of three objective functions are presented in Table3.

The comparison results of the experiment on the real robot applying angle from trial-and-error and MOWOA techniques can be discussed as follows. For the orbital energy, the MOWOA achieves better result over the trial-and-error for 16.11%. For the phase portrait aspect, the MOWOA conducts better results over the trial-and-error for 6.46%. This means the MOWOA gives a smoother movement of COG. For the jerk analysis, the MOWOA demonstrates better results of 54.84%. This means it can prevent the damage on joint 54.84% over the trial-and-error technique. All comparison results are shown in

Table4. The comparison results of jerk are show in Fig. 15 and Fig. 16.

TABLE III. RESULT OF RECOVER TECHNIQUES OF PATTERN GENERATORS OF HUMANOID ROBOT IN OBJECTIVE FUNCTION.

Objective function	Simulation	Actual*	Trial-and-error
Orbital Energy	3,219,129.50	**2,863,521.26**	3,413,651.50
Error of phase portrait	**4,046.05 mm²/s**	7,611.52 mm²/s	8,137.53 mm²/s
Jerk	47,385.65 degree/sec³	**41,464.18 degree/sec³**	91,835.68 degree/sec³

*Actual means the test on real robot

TABLE IV. THE COMPARISON ERROR OF RESULT TECHNIQUES OF PATTERN GENERATORS OF HUMANOID ROBOT IN OBJECTIVE FUNCTION.

Objective function	Simulation VS Actual	Simulation VS Trial-and-error	Actual VS Trial-and-error
Orbital Energy	11.04%	6.04%	**16.11%**
Error of phase portrait	46.84%	50.27%	**6.46%**
Jerk	12.49%	48.40%	**54.84%**

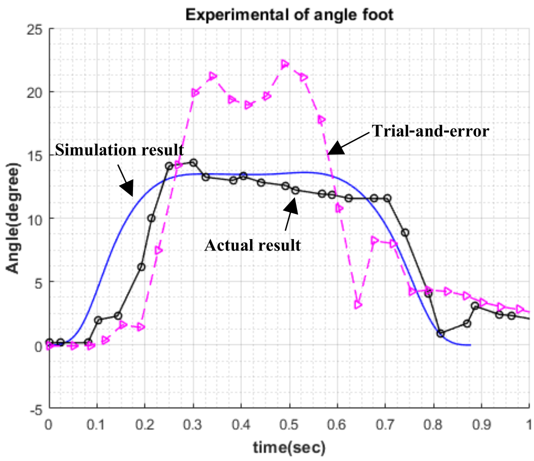

Figure 12 Comparison results of angle foot for 3 techniques.

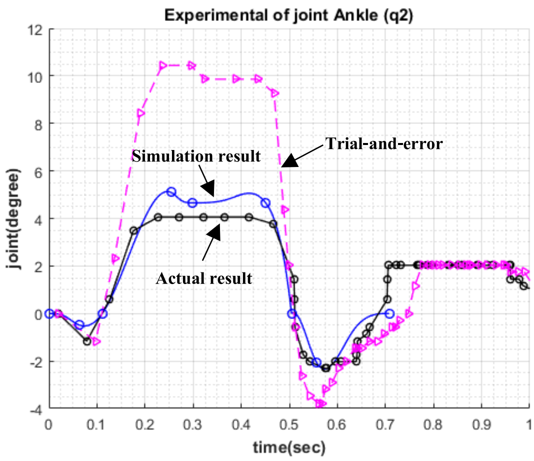

Figure 13. Comparison result of right ankle for 3 techniques.

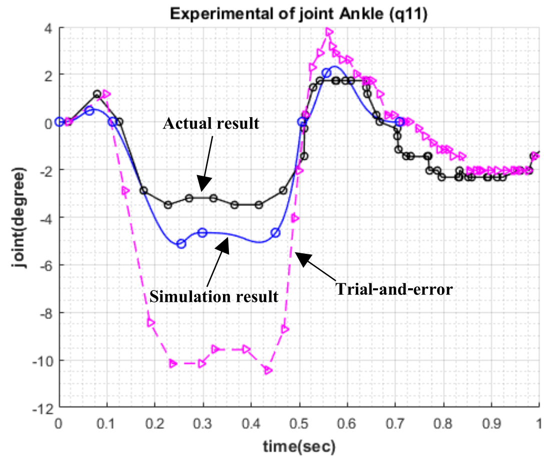

Figure 14. Comparison result of left ankle for 3 techniques.

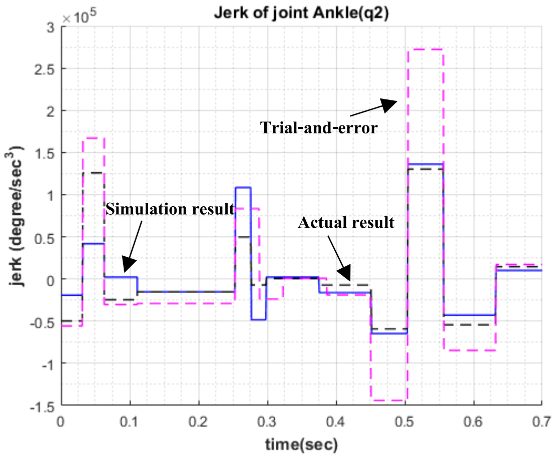

Figure 15. Comparison of jerk for right ankle.

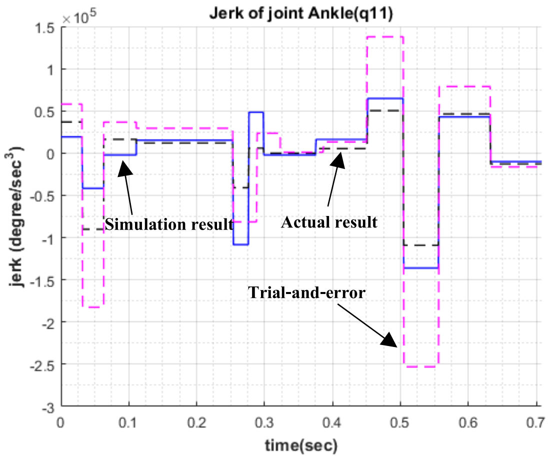

Figure 16. Comparison of jerk for left ankle.

The analysis result of the COG position must be considered to indicate robot's stability. The angle of foot and joint ankles are utilized to determine the COG position, as show in Fig 17. From the experiment, it is found that changing of COG position can be separated into 4 main parts which are; 1) "Part A" it is the period that the robot received external force and its gesture is a controlled response through the joint ankle for 4.93 degree. "Part B" is the period of delay time of joint ankle and control joint ankle to the initial position. At this stage, the robot start to hold its position. “Part C” is the period when the robot moves forward according to the gravity. “Part D” is the period when the robot entered into stagnant state. This position average minimum COG position of the MOWOA simulation is 17.13 mm (0 mm is unstable), the MOWOA on real robot is 12.54 mm and the trial-and-error is 2.83 mm. This means the trial-and-error is closer to unstable state.

For all results, they demonstrate that the techniques of optimization by MOWOA can solve complexity problem, such a humanoid robot, better than trial-and-error.

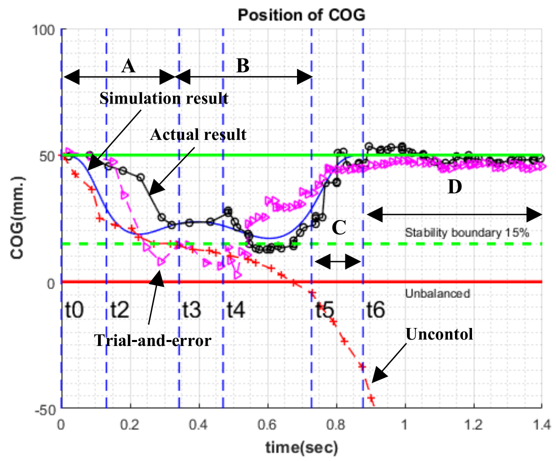

Figure 17. The experimental trajectory of COG.

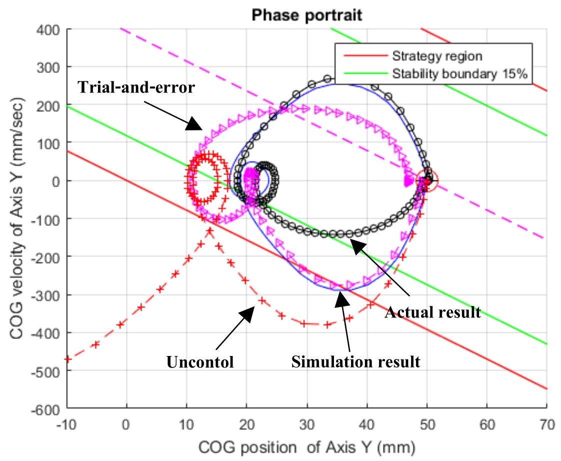

Figure 18. The experimental trajectory of COG on phase portrait.

V. Conclusion

The balancing humanoid robot from external force is an important and can be application in the future when human and humanoid are working together. This is because the large force causing the robot falling over damaged or even dangerous to human. This work focuses on recovery strategy balancing of a Bioloid robot from external force (1.11N) by controlling robot’s joint. There are 12 joints that are important to balance humanoid robot. Each joint of the robot has differences in weight and position. As this research focuses to restore robot balancing, an ankle joint control strategy is chosen from six strategies which are; 1) ankle strategy, 2) knee strategy, 3) ankle and knee strategy, 4) ankle and hip strategy, 5) ankle, knee and hip strategy, and 6) whole body (ankle, knee, hip and arms) strategy.

The desired recovery trajectory is first obtained from a trial-and-error technique. Later, the Multi-Objective Whale Optimization Algorithm (MOWOA) is used to refine the trajectory. Three objective functions which are; 1) the minimal orbital energy, 2) the minimal error of phase portrait, and 3) the minimal jerk of the joint, are employed. The first objective function indicates that how fast the robot can recover its balance while the second the minimal error of phase portrait shows the smoothness of the COG movement. The last objective function applied for preventing the damage in each joint. This Multi-objective utilizes non-dominated solution for Pareto front and for the decision making, the weighted product method (WPM) is employed. After getting the optimum point in each strategy, the results are then compared to obtain the best strategy which is the Ankle strategy. The mathematical model of the humanoid is developed in the MATLAB to determine position of COG. The data in the estimation of MOWOA obtain the trial-and-error technique for a balance recovering path. The MOWOA shows that the ankle strategy gives the best result with the joint ankle at 4.93 degree and angle foot 13.482 degree.

The experiments show result of 3 techniques which are; 1) the result from trial-and-error technique, 2) the result from the best of optimum point simulation of Ankle strategy by MOWOA and, 3) the actual result on the Bioloid using the value from the simulation. For the orbital energy, the MOWOA achieves better result over the trial-and-error for 16.11%. For the phase portrait aspect, the MOWOA conducts better results over the trial-and-error for 6.46%. This means the MOWOA gives a smoother movement of COG. For the jerk analysis, the MOWOA demonstrates that it can prevent the damage on joint better than the trial-and-error technique 54.84%.

Conflict of Interest

The authors declare no conflict of interest.

Author Contributions

Kittisak Sanprasit and Pramin Artrit designed the model, conducted the experiments, obtained, and analyzed data. Authors had approved the final version.

Acknowledgment

This work was supported by Robotic Engineering Research Laboratory, Department of Electrical Engineering, Faculty of Engineering, Khon Kaen University and Loei Rajabhat University.

References

[1] Jung-Yup Kim, Ill-Woo Park, and Jun-Ho Oh, “Walking control algorithm of biped humanoid robot on uneven and inclined floor,” *Journal of Intelligent & Robotic Systems*, vol. 48, pp. 457-484, January 2007.

[2] Hayder F. N. Al-Shuka, F. Allmendinger, B. Corves, and Wen-Hong Zhu, “Modeling, stability and walking pattern generators of biped robots: a review,” *Robotica*, vol. 32, pp. 907–934, September 2014.

[3] R. Tajima, D. Honda, and K. Suga, “Fast running experiments involving a humanoid robot,” in *Proc. IEEE International Conf. Robotics and Automation*, Kobe Japan, pp. 1571-1576, 2009.

[4] S. Sakka, and K. Yokoi, “Humanoid vertical jumping based on force feedback and inertial forces optimization,” in *Proc. IEEE International Conf. Robotics and Automation*, Barcelona, Spain , pp. 3752-3757, 2005.

[5] N. Sawasaki, T. Nakajima, and A. Shiraishi, “Application of humanoid robots to building and home management services,” in *Proc. IEEE International Conf. Robotics & Automation*, Taipel, Taiwan, pp. 2992-2997, 2003.

[6] H. Hasunuma et al., “A tele-operated humanoid robot drives a lift truck,” in *Proc. IEEE International Conf. Robotics & Automation*, Washigton, DC, USA, pp. 2246-2252, 2002.

[7] B. Stephens, “Humanoid push recovery,” in *Proc. IEEE-RAS International Conf. Humanoid Robots*, Pittsburgh, USA, pp. 589-595, 2007.

[8] Sang-Ho Hyon and G. Cheng, “Disturbance rejection for biped humanoids,” in *Proc. IEEE International Conf. Robotics and Automation*, Roma, Italy, pp. 2668-2675, 2007

[9] H. Ono, T. Sato, and K. Ohnishi, “Balance recovery of ankle strategy: Using knee joint for biped robot,” *International Symposium on Access Spaces (ISAS)*, pp. 17-19, 2011.

[10] S. Kiemel, “Balance maintenance of a humanoid robot using the hip-ankle strategy,” M.S. thesis, Dept. Mechanical, Maritime and Materials Eng., Delft University of Technology. Delft, Netherlands, 2012.

[11] M. Nakada, B. Allen, S. Morishima, and D. Terzopoulos, “Learning arm motion strategies for balance recovery of humanoid robots,” *IEEE International Conf. Emerging Security Technologies* . Canterbury, UK, pp. 165-170, 2010.

[12] Thi-Kien Dao, Tien-Szu Pan, and Jeng-Shyang Pan, “A multi-objective optimal mobile robot path planning based on whale optimization algorithm,” *IEEE International Conf. Signal Processing (ICSP)*, Chengdu, China, pp. 337-342, 2016.

[13] J. Z. Wang, P. Du, Tong and Niu, W. D. Yang, “A novel hybrid system based on a new proposed algorithm-multi-objective whale optimization algorithm for wind speed forecasting,” *Applied Energy*, vol. 208. pp. 344-360, October 2017.

[14] G. O. Odu, O. E. Charles-Owaba, “Review of multi-criteria optimization methods-theory and applications,” *IOSR Journal of Engineering (IOSRJEN)*, pp. 1-14, October 2013.

[15] R. N. Jazar, *Theory of Applied Robotics*, 2nd ed. New York, USA. : Springer, 2010.

[16] J. V. Nunez, A. Briseno, D. A. Rodriguez, J. M. Ibarra, and V. M. Rodriguez, “Explicit analytic solution for inverse kinematics of Bioloid humanoid robot,” *Brazilian Robotics Symposium and Latin American Robotics Symposium*, pp.33-38, 2012.

[17] K. Omar et al., “Kinematic modeling of a humanoid soccer–player: Applied to BIOLOID premium type a robot,” in *Intelligent Robotics Systems : Ispiring the NEXT : 16th FIRA RoboWorld Congress, FIRA 2013*, Kuala Lumpur, Malaysia. London : springer, pp. 49-63, 2013.

[18] M. W. Spong, S. Hutchinson, and M. Vidyasagar, *Robot Modeling and Control*, 1st ed, New York : John Wiley & Sons, Inc. N.d..

[19] D. A. Winter, *Biomechanics and Motor Control of Human Movement*, 4th ed, New Jersey : John Wiley & Sons, Ins, 2009.

[20] B. Stephens, “Push recovery control for force-controlled humanoid robot,” Ph.D. dissertation. The Robotics Institute Carnegie Mellon University Pittsbrgh, Pennsylvania, USA., 2011.

[21] L. Biagiotti, and C. Melchiorri, *Trajectory Planning for Automatic Machines and Robots*, Berlin Heidelbeng : Springer, 2008.

[22] K. Y. Kim and J. H. Park, “Ellipse-based leg-trajectory generation for galloping quadruped robot,” *Journal of Mechanical Science and Technology*, vol. 22, pp. 2099-2106, July 2008.

[23] S. Kajita, H. Hirukawa, K. Harada, and K. Yokoi, *Introduction to Humanoid Robotics*, Heidelberg : Springer, 2014.

[24] P. Tangpattanakul, A. Meesomboon, and P. Artrit, “Optimal trajectory of robot manipulator using harmony search algorithms,” in *Recent Advances in Harmony Search Algorithm*. Virginia : Springer, pp. 23-36, 2010.

[25] I. R. Kumawat, S. J. Nanda, “Multi-objective whale optimization,” in *Proc. IEEE TENCON Conf.* Penang, Malaysia, pp. 2747-2752, 2017.

[26] S. Mirjalili, S. Saremi, S. M. Mirjalili, and L. dos S. Coelho. “Multi-objective grey wolf optimizer: A novel algorithm for multi-criterion optimization,” *Expert Systems With Applications*, vol. 47, pp.106-119, 2016.

[27] K. Nuaekaewa, P. Artrit, N. Pholdee, S. Bureerat, “Optimal reactive power dispatch problem using a two-archive multi-objective grey wolf optimizer,” *Expert Systems With Application*, vol 87, pp. 79-89, June 2017.

[28] S. Mirjalili, A. Lewis, “The whale opitmization algorithm,” *Advances in Engineering Software*, vol. 95, pp. 51-67 January 2016.

Kittisak Sanprasit received his M.Sc. degree in Computer Science from King Mongkut’s University of Technology North Bangkok in 2008. Currently he is pursuing his Ph.D. degree in Dept. of Electrical Engineering, Faculty of Engineering, Khon Kaen University, Khon Kaen, Thailand.

Pramin Artrit received his Ph.D. degree in Advanced Robotics from University of Salford, U.K., in 2004. He is currently working as an Assistant Professor at Department of Electrical Engineering, Faculty of Engineering, Khon Kaen University, Khon Kaen, Thailand. His research interests include control systems and automation, bipedal walking and balancing robot.

APPENDIX A: DH PARAMETER TABLE

TABLE A.1 DH PARAMETER TABLE FROM POINT REFERENT (A) TO POINT JOINT RIGHT ANKLE (V)

Frame No.	θ_i	d_i	a_i	α_i
V1	pi/2	LF0	LF1	0
V2	pi+q_f	0	LF1	0
V3	pi+q_b	0	LF2	pi/2
V4	0	0	0	pi/2
V5	pi/2	0	RL1	pi/2

TABLE A.2 DH PARAMETER TABLE FROM POINT JOINT LEFT ANKLE (V) TO END EFFECTOR OF LEFT HEEL (F)

Frame No.	θ_i	d_i	a_i	α_i
1	q_1	0	0	-pi/2
2	q_2+$q_{i2,3}$	0	RL2	0
3	q_3-$q_{i3,4}$	0	RL3	0
4	q_4+$q_{i4,5}$	0	0	pi/2
5	q_5	0	RL4	pi/2
6	pi/2	0	0	-pi/2
7	q_6-pi/2	0	-RL5	0
8	q_7	LL4	0	pi/2
9	q_8+pi/2	0	0	-pi/2
10	q_9-$q_{i9,10}$	0	LL3	0
11	q_{10}+$q_{i10,11}$	0	LL2	0
12	q_{11}-$q_{i11,12}$	0	0	pi/2
13	q_{12}	0	LL1	0
14	0	LF2	0	0

TABLE A.3 DH PARAMETER TABLE FROM POINT JOINT RIGHT HIP (q_6) TO POINT EFFECTOR OF HEAD (H)

Frame No.	θ_i	d_i	a_i	α_i
V6	q_6-pi/2	0	-B1	0
V7	0	-B2	0	0
V8	0	-B3	0	0

TABLE A.4 DH PARAMETER TABLE FROM CENTER OF BODY (TORSO) TO POINT EFFECTOR OF RIGHT HAND (R)

Frame No.	θ_i	d_i	a_i	α_i
15	0	0	0	pi/2
16	pi/2	0	0	pi/2
17	0	D1	0	0
18	q_{13}	D2	D3	pi/2
19	q_{14}	0	D4	0
20	q_{15}	0	D5	0

TABLE A.5 DH PARAMETER TABLE FROM CENTER OF BODY (TORSO) TO POINT EFFECTOR OF LEFT HAND (L)

Frame No.	θ_i	d_i	a_i	α_i
21	0	0	0	pi/2
22	pi/2	0	0	pi/2
23	0	-A1	0	0
24	q_{16}	-A2	A3	pi/2
25	q_{17}	0	A4	0
26	q_{18}	0	A5	0

TABLE A.6 DH PARAMETER TABLE OF SUB MASS

Frame No.	θ_i	d_i	a_i	α_i	Pcom
C1	0	L1COM	L2COM	0	Pcom1
C2	$q_2+q_{i2,3}$	0	L3COM	0	Pcom2
C3	$q_4+q_{i4,5}$	0	0	pi/2	Pcom3
C4	0	L4COM	L5COM	0	
C5	0	0	0	pi/2	Pcom4
C6	0	-L6COM	-L7COM	0	
C7	0	0	-L8COM	0	Pcom5
C8	0	-L9COM	-L10COM	0	Pcom6
C9	q_6-pi/2	0	-L11COM	0	Pcom7
C10	0	-L12COM	0	0	
C11	0	0	0	pi/2	
C12	0	L13COM	0	0	
C13	q_{14}	0	L14COM	0	Pcom8
C14	q_{15}	0	L15COM	0	Pcom9
C15	q_{17}	0	L16COM	0	Pcom10
C16	q_{18}	0	L17COM	0	Pcom11

APPENDIX B: VARIABLE AND CONSTANTS

TABLE B VARIABLE AND CONSTANTS

Number	variable	Constants	Number	variable	Constants
1	LF0	110 mm.	14	A3,D3	14.5 mm.
2	LF1	100 mm.	15	A4,D4	67.5 mm.
3	LF2	50 mm.	16	A5,D5	106 mm.
4	RL1,LL1	31 mm.	17	L1COM,L9COM	-16.56 mm.
5	RL2,LL2	74 mm.	18	L2COM,L10COM	11.68 mm.
6	RL3,LL3	74 mm.	19	L3COM,L8COM	63.41 mm.
7	RL4,LL4	29 mm.	20	L4COM,L6COM	-18.25 mm.
8	RL5	80 mm.	21	L5COM,L7COM	-17.96 mm.
9	B1	40 mm.	22	L11COM	40.7 mm.
10	B2	31 mm.	23	L12COM	52.1 mm.
11	B3	49 mm.	24	L13COM	12.25 mm.
12	A1, D1	47 mm.	25	L14COM,L16COM	23.43 mm.
13	A2, D2	2 mm.	26	L15COM,L17COM	35.86 mm.

APPENDIX C: POSITION AND THE MASS OF EACH LINK

TABLE C POSITION AND THE MASS OF EACH LINK

mass	weight(kg.)	axis x (mm.)	axis y (mm.)	axis z (mm.)
M1	0.172	110	33.440	42.680
M2	0.083	110	92.549	78.014
M3	0.166	110	31.627	142.690
M4	0.166	30	33.440	42.680
M5	0.083	30	92.549	78.014
M6	0.172	30	31.627	142.690
M7	0.582	69.3	48.387	240.506
M8	0.078	142.310	66.090	237.197
M9	0.078	154.951	69.435	159.121
M10	0.078	-2.313	66.090	237.197
M11	0.078	-14.965	69.435	159.121
total mass	1.736			
position		69.746	49.892	159.450